JOURNAL OF MATERIALS SCIENCE **36** (2001) 1099–1104

Defect structure and ionic conductivity as a function of thermal history in BIMGVOX solid electrolytes

I. ABRAHAMS*
Structural Chemistry Group, Queen Mary and Westfield College, Mile End Road, London E1 4NS, UK
E-mail: I.Abrahams@qmw.ac.uk

F. KROK*, M. MALYS
Faculty of Physics, Warsaw University of Technology, ul. Koszykowa 75, 00662 Warsaw, Poland

A. J. BUSH‡
Structural Chemistry Group, Queen Mary and Westfield College, Mile End Road, London E1 4NS, UK

The defect structure of the oxide ion conducting solid electrolyte, Mg substituted $Bi_4V_2O_{11-\delta}$ (BIMGVOX), was examined by high-resolution powder neutron diffraction. A detailed explanation of interpretation of the defect structure is presented. The general formula for the BIMGVOX solid solutions $Bi_2V_{1-x}Mg_xO_{5.5-3x/2}$ assumes complete oxidation of vanadium to $V^{V.}$ Analysis of the neutron diffraction data reveals the defect structure and indicates that there is, in fact, partial reduction of vanadium to V^{IV}. The extent of reduction is dependent on thermal history, with high temperature quenched samples showing a greater degree of reduction than exponentially slow cooled samples. This is correlated with differences in electrical behaviour at low and high temperatures. Differences in ionic conductivity and activation energies between samples with different thermal histories are explained in terms of the balance between charge carrier concentration and the extent of defect trapping effects.

1. Introduction

The BIMEVOXes are a group of fast oxide ion conducting solid electrolytes based on aliovalent substitution in the parent compound $Bi_4V_2O_{11-\delta}$ [1–3]. Their interest lies in excellent ionic conductivities, particularly at low and intermediate temperatures, which can be in the range of 10^{-3} S cm^{-1} at 300 °C and 10^{-1} S cm^{-1} at 600 °C [4]. The divalent substituted materials have been studied extensively [4], and have a general solid solution formula $Bi_2V_{1-x}M^{II}{}_xO_{5.5-3x/2-\delta}$ (where M^{II} is a divalent metal). Apart from having their own applications in low-temperature electrochemical gas separation membranes [5], the BIMEVOXes also serve as model compounds for understanding processes common to all oxide ion conducting solid electrolytes.

The structure of the parent compound $Bi_4V_2O_{11-\delta}$ is made up of alternating layers of $[Bi_2O_2]_n^{n2+}$ and $[VO_{3.5-\delta}\square_{0.5+\delta}]_n^{n2-}$ (where □ represents an oxide ion vacancy). Polymorphism arises due to ordering of vacancies in the vanadate layer with three principal polymorphs (α, β and γ) stable over various temperature ranges [3]. The fully disordered tetragonal γ-phase is stabilised to room temperature on substitution of vanadium by aliovalent metal atoms and it is this phase that exhibits the high ionic conductivities that are characteristic of these materials.

An idealised model for the structure of γ-$Bi_4V_2O_{11-\delta}$ is shown in Fig. 1. Bismuth is in square pyramidal coordination with oxygen, while the Bi $6s^2$ lone pairs are stereochemically active and point towards the vanadate layers above and below. In the idealised case V can be thought of as octahedrally coordinated to oxygen. However, high concentrations of oxide ion vacancies in the vanadate layer and simple stoichiometric considerations preclude exclusive occurrence of vanadium octahedra. Neutron diffraction studies on the Co and Ni substituted systems have confirmed that vacancies are mainly concentrated in the 'equatorial' oxide positions [6–8]. In addition these studies have shown extensive distortion of the vanadium polyhedra. Careful analysis of the diffraction results has allowed us to propose a model for the defect structure of divalent substituted

* Authors to whom all correspondence should be addressed.
‡ *Present Address*: Johnson Matthey, Catalytic Systems Division, Orchard Road, Royston, Herts SG8 5HE, UK.

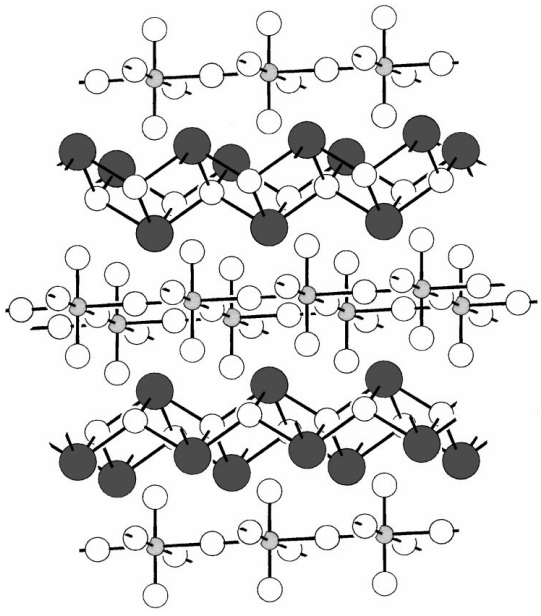

Figure 1 Idealised structure for $Bi_4V_2O_{11-\delta}$ showing Bi (filled circles), V (shaded circles) O (open circles) atoms. Oxygen vacancies are omitted for clarity.

BIMEVOXes with two principal coordination environments viz: distorted tetrahedral and distorted octahedral (Fig. 2). At the $x = 0.10$ composition the ratio of tetrahedra to octahedra is approximately 2 : 1 [7, 8]. ^{51}V solid state NMR studies on the parent compound, $Bi_4V_2O_{11-\delta}$, confirms the occurrence of these two principal coordination environments for vanadium [9].

Electrical studies on γ-phase BIMEVOXes using ac impedance spectroscopy have generally shown two linear ranges in their Arrhenius plots of conductivity, one at low temperatures and one at high temperatures [10–13]. The high temperature region, above ca. 500 °C, is characterised by low activation energies, ca 0.5 eV, and high conductivities, in the order of 10^{-1} S cm^{-1} at 600 °C. The low temperature region has higher activation energies, ca 0.7 eV, and conductivities in the order of 10^{-3} S cm^{-1}. While the high temperature region is associated with the fully disordered γ-phase, the change in activation energy on thermal cycling has been interpreted as occurring through an ordering of vacancies in the vanadate layer. This partially ordered γ-phase is indistinguishable through X-ray powder diffraction analysis from the fully disordered phase. However, using high-resolution powder neutron diffraction a weak incommensurate superstructure was detected in the case of the cobalt substituted system [10, 14]. This modulated incommensurate phase has been termed γ'. The γ'-modulation occurs in samples that are slow cooled after high temperature synthesis or subject to prolonged heating at intermediate temperatures, for example during the course of temperature dependent conductivity measurements [15]. This ordering phenomenon must be related to ordering of the vanadium polyhedra in the vanadate layer. Vanadium oxides with vanadium nominally in the 5+ oxidation state generally show a degree of inherent reduction to V^{IV}. This general observation combined with the fact that the appearance of the γ'-phase is connected to time dependent thermal history, suggests that vanadium reduction and the consequent change in vacancy concentration also have significant roles in the formation of the modulated γ'-phase. We have previously shown that vanadium reduction results in weak paramagnetic behaviour in the parent compound $Bi_4V_2O_{11-\delta}$ [9].

The Mg doped system, BIMGVOX, shows an extensive range of solid solutions [13]. The use of a non-reducible main group substituent ion, such as magnesium, allows for a study of the defect structure as a function of vanadium reduction, independent of possible reduction of the substituent ion. Here we present electrical and structural results, obtained by ac impedance spectroscopy and high-resolution powder neutron diffraction respectively, for $Bi_2V_{0.9}Mg_{0.1}O_{5.35-\delta}$.

2. Experimental

2.1. Preparations

Samples of $Bi_2V_{0.9}Mg_{0.1}O_{5.35-\delta}$ were prepared by conventional solid state synthesis using procedures described previously for other members of the BIMEVOX family [16]. A starting mixture of Bi_2O_3 (POCh, 99.9%), MgO (POCh, 99.5%) and V_2O_5 (ABCR, 99.5%) was used. The ground mixture was heated initially at 620 °C for 12 h cooled, reground and pelletised. Pellets were then sintered at 850 °C for 5 h. Samples were then either quenched in air to room

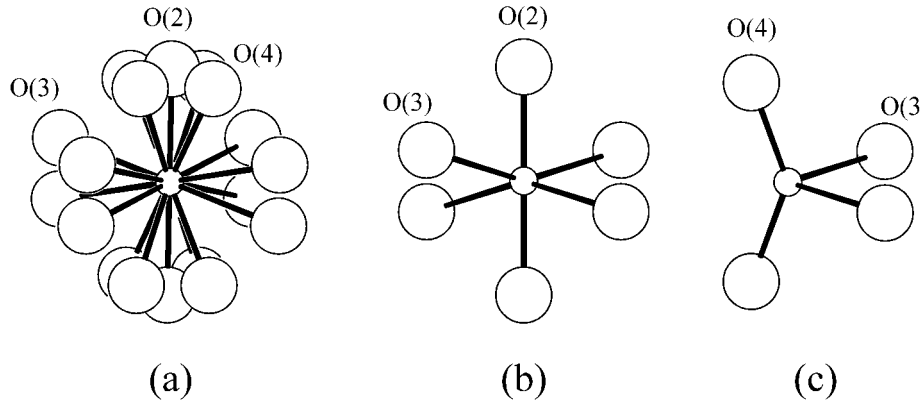

Figure 2 Vanadium coordination polyhedra in γ-BIMEVOX: (a) average crystallographic vanadium environment (b) derived distorted octahedron and (c) derived distorted tetrahedron.

temperature, to preserve the high temperature structure, or slow cooled exponentially, to allow structural relaxation.

2.2. Electrical measurements

Electrical parameters were determined by ac impedance spectroscopy over the temperature range 150 to 730 °C using a Solartron 1255/1286 system in the frequency range 1 Hz to 5×10^5 Hz. Samples for impedance measurements were prepared as rectangular blocks (ca $6 \times 3 \times 3\ mm^3$) cut from slow cooled sintered pellets using a diamond saw. Platinum electrodes were sputtered by cathodic discharge. Impedance measurements were carried out over two cycles of heating and cooling. In order to observe the effect of quenching, just prior to measurement, some pellets were heated to 700 °C overnight and quenched in air to room temperature.

2.3. Neutron Diffraction

High-resolution powder neutron diffraction data were collected on the HRPD diffractometer at the ISIS facility, Rutherford Appleton Laboratory. Data were collected at room temperature in back-scattering mode over the time of flight range 30–130 ms. The sample was located in a vanadium can, 1 m in front of the back-scattering detectors. Data were collected on quenched and slow cooled samples.

Structure refinement was carried out by the Rietveld method using the GSAS suite of programs [17]. A structure based on that of BICOVOX [7] was used as an initial model. Isotropic thermal parameters were refined for all atoms with those of O(2) and O(4) tied together due to the close proximity of these sites to one another. O(2) and O(4) cannot be simultaneously occupied and their occupancies are also related to the occupancy of the 'equatorial' site O(3). A linear constraint was therefore applied to the occupancy parameters of O(2), O(4) and O(3) (see below). Refinement and crystal parameters are summarised in Table I.

TABLE I Crystal and refinement parameters for $Bi_2V_{0.9}Mg_{0.1}O_{5.35-\delta}$

	Quenched	Slow cooled
Formula	$Bi_2V_{0.9}Mg_{0.1}O_{5.274}$	$Bi_2V_{0.9}Mg_{0.1}O_{5.310}$
M	550.62	551.20
Crystal system	Tetragonal	Tetragonal
Space group	I4/mmm	I4/mmm
Cell dimensions (Å)	$a = 3.93535(5)$, $c = 15.4489(2)$ Å	$a = 3.93278(5)$ $c = 15.4417(2)$ Å
Vol. (Å^3)	239.257(10)	238.833(9)
Z	2	2
D_c (g cm^{-3})	7.646	7.667
Appearance	Dark brown powder	Orange brown powder
Temperature	298 K	298 K
Data range collected	30–130 ms	30–130 ms
Data range refined	34–118 ms	34–118 ms
No. of data points	4148	6221
No of variables	24	24
R-factors	$R_p = 0.0711$, $R_{wp} = 0.0791$, $\chi^2 = 14.79$	$R_p = 0.0679$, $R_{wp} = 0.0643$, $\chi^2 = 6.08$

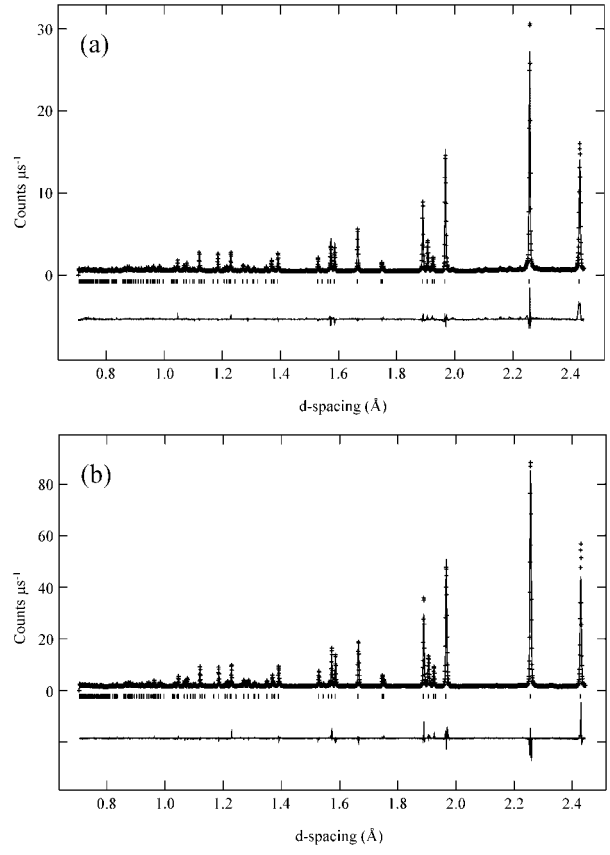

Figure 3 Fitted diffraction profiles for $Bi_2V_{0.9}Mg_{0.1}O_{5.35-\delta}$ (a) quenched from 850 °C and (b) slow cooled from 850 °C, showing observed (points), calculated (line) and difference (lower) profiles. Markers indicate reflection positions.

3. Results and discussion

The diffraction patterns of the quenched and slow cooled materials look very similar and in both cases all peaks can be indexed in the tetragonal space group I4/mmm (no. 139 [18]). Table II summarises the final refined structural parameters of the quenched and slow cooled samples, with the corresponding fitted diffraction profiles shown in Fig. 3. The basic structural features are common to other BIMEVOXes and have already been described in the introduction. Of particular interest in this study is the disorder in the vanadate layer. Vanadium and magnesium atoms share the metal atom site, M, in the vanadate layer. Due to the relatively poor scattering of neutrons by vanadium it is impossible to say if there is any significant displacement of scattering density away from the idealised 2b site used in the model. Three oxygen sites were modelled in the vanadate layer; O(2) and O(4) are the nominal 'apical' positions while O(3) is the nominal 'equatorial' site (Fig. 2).

Both O(2) and O(4) sites are non-bridging. O(2) is a four-fold site in the ideal apical position for a vanadium/magnesium (M) octahedron. O(4) is a sixteen-fold site and is associated exclusively with distorted tetrahedral coordination for M. Independent refinement of O(2) and O(4) fractional occupancies always resulted in a total 'apical' oxygen per M atom

TABLE II Final refined atomic parameters for $Bi_2V_{0.9}Mg_{0.1}O_{5.35-\delta}$

Atom	Site	*x*	*y*	*z*	Occupancy	U_{iso} (Å^2)
(a) Quenched						
Bi	4e	0.0(−)	0.0(−)	0.16917(7)	1.0(−)	0.0385(5)
V/Mg	2b	0.5(−)	0.5(−)	0.0(−)	0.9/0.1(−)	0.025(−)
O(1)	4d	0.0(−)	0.5(−)	0.25(−)	1.0(−)	0.0342(6)
O(2)	4e	0.5(−)	0.5(−)	0.1097(8)	0.279(10)	0.057(2)
O(3)	8g	0.5(−)	0.0(−)	0.0295(3)	0.319(8)	0.087(2)
O(4)	16n	0.5(−)	0.3160(24)	0.0920(4)	0.180(3)	0.057(2)
(b) Slow cooled						
Bi	4e	0.0(−)	0.0(−)	0.16942(5)	1.0(−)	0.0359(4)
V/Mg	2b	0.5(−)	0.5(−)	0.0(−)	0.9/0.1(−)	0.025(−)
O(1)	4d	0.0(−)	0.5(−)	0.25(−)	1.0(−)	0.0343(4)
O(2)	4e	0.5(−)	0.5(−)	0.1049(5)	0.315(6)	0.065(1)
O(3)	8g	0.5(−)	0.0(−)	0.0316(2)	0.328(4)	0.075(1)
O(4)	16n	0.5(−)	0.2290(17)	0.0897(3)	0.171(1)	0.065(1)

ratio of 2 : 1 or greater. This suggests that there are no nominal 'apical' vacancies in the system and that each M atom is coordinated to either two O(2) or two O(4) atoms. On a particular oxygen site *m*, the fractional occupancy per M atom can be defined as $F_{O(m)}$. An O(2) : O(4) ratio higher than 2 : 1 is physically impossible, since both sites cannot be simultaneously occupied due to their close proximity; consequently the following relationship holds:

$$F_{O(2)} + F_{O(4)} = 2 \tag{1}$$

O(3) is situated slightly above and below the ideal 'equatorial' plane and is a bridging atom common to both octahedral and tetrahedral M-atom coordinations. Therefore the total occupancy of O(3) per M atom, $F_{O(3)}$, is the sum of an octahedral contribution, $F_{O(3oct)}$ and a tetrahedral contribution $F_{O(3tet)}$, i.e.:

$$F_{O(3)} = F_{O(3oct)} + F_{O(3tet)} \tag{2}$$

The individual contributions, $F_{O(3oct)}$ and $F_{O(3tet)}$, may be calculated from a consideration of the ratios of non-bridging to bridging atoms in the respective M-atom polyhedra. Each octahedrally coordinated M-atom is bonded to two non-bridging O(2) and four bridging O(3) atoms, giving ratios M : O(2) = 1 : 2 and M : $O(3_{oct})$ = 1 : 2 (each bridging atom contributes 0.5 per M atom). Therefore as the ratio O(2) : $O(3_{oct})$ is 1 : 1,

$$F_{O(3oct)} = F_{O(2)}. \tag{3}$$

Similarly for tetrahedral coordination, each M-atom is bonded to two O(4) non-bridging atoms and two bridging O(3) atoms, i.e., ratios M : O(4) = 1 : 2 and M : O(3tet) = 1 : 1. Therefore, O(4) : O(3tet) = 2 : 1 and,

$$F_{O(3tet)} = F_{O(4)}/2. \tag{4}$$

The relationships given in Equations 1 and 2 enabled a linear constraint to be refined in the model, tying the fractional occupancies of O(2), O(4) and O(3) to a single variable. The relative fractions of M sites that are tetrahedral, X_{tet}, and octahedral, X_{oct}, can be calculated as follows:

$$X_{oct} = F_{O(2)}/2 = F_{O(3oct)}/2 \tag{5}$$

$$X_{tet} = F_{O(4)}/2 = F_{O(3tet)} \tag{6}$$

Assuming that Bi is only present in the trivalent state (which is evident by the coordination adopted), the overall charge on the $[V_{0.9}Mg_{0.1}O_{3.35-\delta}]_n$ layer must be $2n-$ to preserve electroneutrality. Taking this into account, and subtracting the contribution to the layer charge from Mg^{2+} (0.2), the effective charge on vanadium, Z_{eff}, may be calculated as follows:

$$Z_{eff} = \frac{2(F_{O(2)} + F_{O(3)} + F_{O(4)}) - 2.2}{0.9} \tag{7}$$

The value of δ in the formula, $Bi_2V_{0.9}Mg_{0.1}O_{5.35-\delta}$, may readily be calculated as follows:

$$\delta = 3.35 - (F_{O(2)} + F_{O(3)} + F_{O(4)}) \tag{8}$$

Table III summarises the $F_{O(m)}$ values and extracted parameters for the quenched and slow cooled samples. It is clear that the effect of slow cooling is to increase the value of $F_{O(2)}$ and $F_{O(3oct)}$ at the expense of $F_{O(4)}$ and $F_{O(3tet)}$, i.e. to decrease the tetrahedral:octahedral site ratio. The difference in Z_{eff} for V is also very significant,

TABLE III M : O ratios and extracted parameters[a] for $Bi_2V_{0.9}Mg_{0.1}O_{5.35-\delta}$

	Quenched	Slow cooled
$F_{O(2)}$	0.558	0.630
$F_{O(3oct)}$	0.558	0.630
$F_{O(3tet)}$	0.720	0.684
$F_{O(3)}$	1.276	1.312
$F_{O(4)}$	1.440	1.368
X_{oct}	0.279	0.315
X_{tet}	0.720	0.684
Z_{eff}	4.831	4.911
δ	0.076	0.040

[a] $F_{O(m)}$ is the fractional occupancy per M atom for oxygen site *m*, X_{oct} and X_{tet} are the fractions of octahedral and tetrahedral M atom coordinations respectively and Z_{eff} is the effective valency of vanadium.

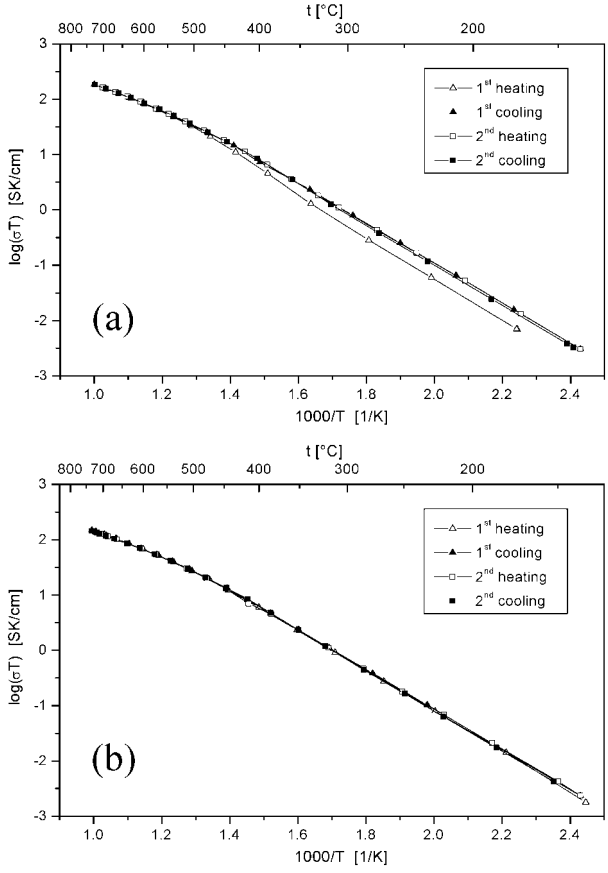

Figure 4 Arrhenius plots of total conductivity for $Bi_2V_{0.9}Mg_{0.1}O_{5.35-\delta}$ (a) quenched from 700 °C and (b) slow cooled from 850 °C.

with the proportion of V^{IV} approximately doubled in the quenched sample. This is correlated to the difference in unit cell volumes, with that of the quenched sample larger than that of the slow cooled, which reflects the larger ionic radius of V^{IV}.

Fig. 4 shows the Arrhenius plots of conductivity for quenched and slow cooled samples of $Bi_2V_{0.9}Mg_{0.1}O_{5.35-\delta}$. While the slow cooled sample shows fully reproducible behaviour on thermal cycling, the quenched sample shows a lower conductivity and higher activation energy, in the low temperature region, on first heating. In subsequent heating and cooling cycles the electrical behaviour is as for slow cooled samples. The observed difference can now be interpreted in the light of the differences in defect structures outlined above. Two principal factors influence ionic conductivity in these systems, viz: (i) the concentration of 'equatorial' oxide ion vacancies which are effectively the charge carriers and (ii) the extent of defect trapping. These two factors have opposite effects on conductivity and it is the balance of the two that governs the magnitude of effective conductivity.

Increasing charge carrier concentration generally has a positive effect on conductivity. Our neutron diffraction results confirm a higher charge carrier (vacancy) concentration in quenched samples. The conduction mechanism in these systems must involve hopping of vacancies between M-tetrahedra and M-octahedra within the vanadate layer. V^V is well known for its variable coordination in oxides, with four, five and six coordination geometries commonly found in the solid state. It is this fact that makes the BIMEVOXes almost unique in their conduction properties at low temperatures. Interestingly, substitution of V by subvalent ions as in the BIMEVOX solid solutions, generally results in lower conductivities, in the high temperature region, than the parent compound $Bi_4V_2O_{11-\delta}$ [9]. Low temperature conductivities are only increased with respect to the parent compound through stabilisation of the fully disordered γ-phase to room temperature. Generally most substituent metals studied prefer octahedral or tetrahedral coordination in an oxide environment and do not have the flexibility of coordination exhibited by V^V. This implies that solid solution formation generally results in an increased defect trapping effect. This argument can be extended to V^{IV}, which being a larger aliovalent metal, compared to V^V, exhibits a preference for octahedral coordination in an oxide environment. Thus, an increase in V reduction results in an increase in defect trapping, yielding lower overall conductivities and higher activation energies, as observed in the present study for quenched samples. This effect is enhanced by crystallographic ordering, which in decreasing entropy raises enthalpy and hence activation energy and there is some evidence for weak superlattice ordering peaks in the neutron diffraction profile of the quenched sample (Fig. 3a). Quenching of BIMEVOX samples does not always result in decreased conductivity. Indeed, for the same substituent concentration in the analogous zinc-substituted system, BIZNVOX, higher conductivities and lower activation energies are observed in quenched samples in comparison to slow cooled samples [12]. In this case neutron diffraction results suggest a much lower extent of V reduction than is observed in the present study [19] and hence the increased carrier concentration dominates the overall conductivity.

4. Conclusions

A combined approach using high-resolution neutron diffraction and ac impedance spectroscopy has allowed for a detailed interpretation of ionic conductivity in the BIMGVOX system. Analysis of the defect structure of quenched and slow cooled samples reveal a significant difference in the extent of V reduction. This difference is evident in the values of δ calculated from the refined structures of 0.074 and 0.040 for the quenched and slow cooled samples respectively. This difference can be correlated with differences in electrical behaviour between samples. The arguments described here should be generally applicable to all BIMEVOXes. In particular tailoring the balance between altering charge carrier concentration and the extent of defect trapping effects is key to the design of BIMEVOX systems with optimum electrical properties.

Acknowledgements

We wish to thank the EPSRC for access to the ISIS facility, Rutherford Appleton Laboratory and for funding a project studentship to AJB. We also gratefully acknowledge the Polish State Committee for Scientific Research for studentship to MM and the Royal Society of Chemistry for a Journals Grant for International Authors.

References

1. F. ABRAHAM, M. F. DEBREUILLE-GRESSE, G. MAIRESSE and G. NOWOGROCKI, *Solid State Ionics* **28–30** (1988) 529.
2. F. ABRAHAM, J. C. BOIVIN, G. MAIRESSE and G. NOWOGROCKI, *Solid State Ionics* **40/41** (1990) 934.
3. G. MAIRESSE, in "Fast Ion Transport in Solids," edited by B. Scrosati *et al.* (Kluwer Academic, Norwell, MA, 1993) p. 271.
4. J. C. BOIVIN and G. MAIRESSE, *Chem. Mater.* **10** (1998) 2870.
5. J. C. BOIVIN, C. PIROVANO, G. NOWOGROCKI, G. MAIRESSE, PH. LABRUNE and G. LAGRANGE, *Solid State Ionics* **113–115** (1998) 639.
6. C. MULLER, M. ANNE, M. BACMANN and M. BONNET, *J. Solid State Chem.* **141** (1998) 241.
7. I. ABRAHAMS, F. KROK and J. A. G. NELSTROP, *Solid State Ionics* **90** (1996) 57.
8. I. ABRAHAMS, J. A. G. NELSTROP, F. KROK and W. BOGUSZ, *Solid State Ionics* **110** (1998) 95.
9. I. ABRAHAMS, A. J. BUSH, F. KROK, G. E. HAWKES, K. D. SALES, P. THORNTON and W. BOGUSZ, *J. Mater. Chem.* **8** (1998) 1213.
10. F. KROK, I. ABRAHAMS, D. G. BANGOBANGO, W. BOGUSZ and J. A. G. NELSTROP, *Solid State Ionics* **86–88** (1996) 261.
11. F. KROK, I. ABRAHAMS, D. BANGOBANGO, W. BOGUSZ and J. A. G. NELSTROP, *Solid State Ionics* **111** (1998) 37.
12. F. KROK, I. ABRAHAMS, A. ZADROZNA, M. MALYS, W. BOGUSZ, J. A. G. NELSTROP and A. J. BUSH, *Solid State Ionics* **119** (1999) 139.
13. F. KROK, I. ABRAHAMS, M. MALYS, W. BOGUSZ, J. R. DYGAS, J. A. G. NELSTROP and A. J. BUSH, *Solid State Ionics*, in press.
14. S. LAZURE, R. N. VANNIER, G. NOWOGROCKI, G. MAIRESSE, C. MULLER, M. ANNE and P. STROBEL, *J. Mater. Chem.* **5** (1995) 1395.
15. F. KROK, M. MALYS, J. R. DYGAS, W. BOGUSZ and I. ABRAHAMS, *Molecular Physics Reports* **27** (2000) 44.
16. F. KROK, W. BOGUSZ, P. KUREK, M. WASIUCIONEK, W. JAKUBOWSKI and J. R. DYGAS, *Mater. Sci. Eng.* **B21** (1993) 70.
17. A. C. LARSON and R. B. VON DREEL, Los Alamos National Laboratory Report N^{o}. LA-UR-86-748, 1987.
18. "International Tables for Crystallography," Vol. A, 3rd ed., edited by T. Hahn (Kluwer Academic Publishers, Dordrecht, The Netherlands, 1992).
19. I. ABRAHAMS and F. KROK, to be published.

Received 1 May
and accepted 12 June 2000